Downloaded from orbit.dtu.dk on: Aug 16, 2022

DTU Library

The reaction rate for dissociative adsorption of N-2 on stepped Ru(0001): Six-dimensional quantum calculations

van Harrevelt, Rob; Honkala, Johanna Karoliina; Nørskov, Jens Kehlet; Manthe, Uwe

Published in:
Journal of Chemical Physics

Link to article, DOI:
10.1063/1.1927513

Publication date:
2005

Document Version
Publisher's PDF, also known as Version of record

Link back to DTU Orbit

Citation (APA):
van Harrevelt, R., Honkala, J. K., Nørskov, J. K., & Manthe, U. (2005). The reaction rate for dissociative adsorption of N-2 on stepped Ru(0001): Six-dimensional quantum calculations. *Journal of Chemical Physics*, *122*(23), 234702. https://doi.org/10.1063/1.1927513

General rights
Copyright and moral rights for the publications made accessible in the public portal are retained by the authors and/or other copyright owners and it is a condition of accessing publications that users recognise and abide by the legal requirements associated with these rights.

- Users may download and print one copy of any publication from the public portal for the purpose of private study or research.
- You may not further distribute the material or use it for any profit-making activity or commercial gain
- You may freely distribute the URL identifying the publication in the public portal

If you believe that this document breaches copyright please contact us providing details, and we will remove access to the work immediately and investigate your claim.

HTML ABSTRACT + LINKS

The reaction rate for dissociative adsorption of N_2 on stepped Ru(0001): Six-dimensional quantum calculations

Rob van Harrevelt[a)]
Theoretische Chemie, Technische Universität München, Lichtenbergstraße 4, D-85747 Garching, Germany

Karoliina Honkala and Jens K. Nørskov
Center for Atomic-Scale Materials Physics, Department of Physics, Technical University of Denmark, DK-2800 Lyngby, Denmark

Uwe Manthe
Theoretische Chemie, Universität Bielefeld, Postfach 100131, D-33501 Bielefeld, Germany and Theoretische Chemie, Technische Universität München, Lichtenbergstraße 4, D-85747 Garching, Germany

(Received 4 March 2005; accepted 13 April 2005; published online 17 June 2005)

Quantum-mechanical calculations of the reaction rate for dissociative adsorption of N_2 on stepped Ru(0001) are presented. Converged six-dimensional quantum calculations for this heavy-atom reaction have been performed using the multiconfiguration time-dependent Hartree method. A potential-energy surface for the transition-state region is constructed from density-functional theory calculations using Shepard interpolation. The quantum results are in very good agreement with the results of the harmonic transition-state theory. In contrast to the findings of previous model calculations on similar systems, the tunneling effect is found to be small. © *2005 American Institute of Physics*. [DOI: 10.1063/1.1927513]

I. INTRODUCTION

The reaction rate is the central quantity in reaction dynamics. For activated processes it is determined by the quantum dynamics in a well-defined region around the transition state. Accurate quantum-mechanical calculations of the reaction rate are therefore possible without solving the full scattering problem. Using the flux correlation approach,[1–3] the dynamics can be restricted to the region in the vicinity of the reaction barrier. This approach has been applied to several gas-phase systems.[4–25] The combination of the flux correlation approach with the multiconfiguration time-dependent Hartree (MCTDH) scheme for efficient multidimensional wave-packet propagation made it possible to study the quantum dynamics of 12-dimensional systems.[20–25] The previous studies show that quantum effects are significant in reactions where hydrogen atoms are transferred. At room temperature the tunneling effect often increases the reaction rate by one order of magnitude. Thus, accurate reaction rate calculations can require a full quantum-mechanical treatment.

While accurate quantum-dynamics calculations for polyatomic reactions in the gas phase have become increasingly available in recent years, reactions on surfaces still pose a challenge. Accurate quantum-mechanical studies of reactions on surfaces have so far been restricted to the most simple examples of surface reactions: dissociative adsorption of H_2, D_2, or HD on various metal surfaces.[26–51] The initial state-selected reactive scattering calculations have deepened the understanding of the reactions of molecules with surfaces. Comparisons between theoretical and experimental results showed that potential-energy surfaces based on density-functional theory (DFT) calculations are sufficiently accurate to provide a realistic description of the reaction dynamics, although the accuracy is much lower than the typical accuracy achievable for gas-phase systems.

Accurate quantum-dynamics calculations have not yet been presented for heavy diatomic or polyatomic molecules on surfaces. However, such calculations are highly desired to deepen the understanding of heterogenous catalysis. An example of a surface reaction that is very important in catalysis is the dissociative adsorption of N_2 on a stepped ruthenium surface. In this reaction the nitrogen bond is broken and two Ru–N bonds are formed. It is the rate-limiting step in the industrial synthesis of ammonia on Ru catalysts.[52] Due to its importance, the N_2-Ru system has been extensively studied experimentally.[53–60] Density-functional theory (DFT) calculations[52,61–65] explored the electronic structure and the reaction path.

Several low-dimensional quantum calculations for dissociation of N_2 on Ru and related systems, employing model potential-energy surfaces, have been presented in the literature.[66–72] These calculations show a significant tunneling effect on the reaction probability. As discussed by Haase *et al.*,[67] the results suggest that at room temperature the reaction is completely dominated by a tunneling mechanism,[67] which is quite surprising for a heavy-atom system. Consequently, transition-state theory (TST) could not be used to estimate the reaction rate.

The present work studies the tunneling effect for N_2 on Ru by performing accurate quantum-mechanical calculations using a realistic potential-energy surface (PES). The flux correlation approach[1–3] is employed to calculate the thermal rate constant and the cumulative reaction probability for dissociative adsorption of N_2 on a stepped Ru(0001) surface. All six

[a)]Electronic mail: rob.v.harrevelt@ch.tum.de

 © 2005 American Institute of Physics

Downloaded 07 Jun 2010 to 192.38.67.112. Redistribution subject to AIP license or copyright; see http://jcp.aip.org/jcp/copyright.jsp

nitrogen degrees of freedom are included in this study, while the positions of the surface atoms are frozen. The possible effect of electron–hole pairs[59] has not been included in the present description. In future work the effect of the motion of the Ru surface will be investigated.[73] The six-dimensional PES in the barrier region is constructed by Shepard interpolation[74,75] of DFT data. As shown in previous work,[25,76] the Shepard interpolation scheme is particularly efficient for the construction of accurate potential-energy surfaces (PESs) in the barrier region. Based on this realistic PES, the effect of tunneling is examined by comparing the reaction rate in the exact quantum-dynamics study with the rate obtained from classical harmonic TST.

II. THEORY

A. Quantum-mechanical calculation of the reaction rate

The quantum-mechanical approach followed in this work has been reviewed in Ref. 24. Here, the general ideas of this approach are briefly summarized. The rate constant k can be expressed as

$$k = \frac{1}{2\pi\hbar Q_r}\int \mathrm{d}E N(E)\exp(-\beta E), \tag{1}$$

where Q_r is the reactants' partition function per unit volume, E is the total energy, $N(E)$ is the cumulative reaction probability (i.e., the sum of the initial state-selected reaction probabilities for all possible initial states), and $\beta = 1/kT$. An exact quantum-mechanical expression for $N(E)$ is given by

$$N(E) = 2\pi^2\hbar^2\ \mathrm{Trace}\{\hat{F}\delta(\hat{H}-E)\hat{F}\delta(\hat{H}-E)\}, \tag{2}$$

where $\hat{F}$ is the operator for the flux through a dividing surface separating the reactants and products. In numerical calculations it is more convenient to work with the so-called thermal flux operator

$$\hat{F}_{\beta_0} = \exp\left(-\tfrac{1}{2}\beta_0\hat{H}\right)\hat{F}\exp\left(-\tfrac{1}{2}\beta_0\hat{H}\right), \tag{3}$$

where the parameter β_0 corresponds to a reference temperature T_0 according to $\beta_0 = 1/kT_0$. For a finite reference temperature the thermal flux operator is a regular operator, in contrast to the singular standard flux operator $\hat{F}$. Equation (2) can be rewritten as

$$N(E) = 2\pi^2\hbar^2\exp(\beta_0 E)\mathrm{Trace}\{\hat{F}_{\beta_0/2}\delta(\hat{H}-E)\hat{F}_{\beta_0/2}\delta(\hat{H}-E)\}. \tag{4}$$

When the trace in Eq. (4) is evaluated employing the eigenstate representation of $\hat{F}_{\beta_0/2}$,

$$\hat{F}_{\beta_0/2} = \sum_m |f_m\rangle f_m \langle f_m|, \tag{5}$$

one obtains

$$\begin{aligned} N(E) &= 2\pi^2\hbar^2\exp(\beta_0 E)\sum_{lm} f_m f_l |\langle f_m|\delta(\hat{H}-E)|f_l\rangle|^2 \\ &= 2\pi^2\hbar^2\exp(\beta_0 E)\sum_{lm} f_m f_l \left|\int_{-\infty}^{\infty}\exp(\mathrm{i}Et/\hbar)O_{lm}(t)\right|^2. \end{aligned} \tag{6}$$

Here, the overlap matrix $O_{lm}(t)$ is given by $O_{lm}(t) = \langle f_l|\exp(-\mathrm{i}\hat{H}t/\hbar)|f_m\rangle$. In summary, the procedure followed to calculate $N(E)$ is to first calculate the eigenstates of $\hat{F}_{\beta_0/2}$ by iterative diagonalization, then propagate them in time, and finally obtain $N(E)$ according to Eq. (6).

The cumulative reaction probability [Eq. (6)] can be written as $N(E) = \sum_{i=1}^{\infty} N_i(E)$,[14] where $N_i(E)$ can be considered as the contribution of the ith vibrational state of the activated complex to $N(E)$. If there are many low-lying vibrationally excited states of the activated complex, then the number of states required to converge the thermal rate constant

$$k = \frac{1}{2\pi\hbar Q_r}\sum_{i=1}^{\infty}\int \mathrm{d}E N_i(E)\exp(-\beta E) \tag{7}$$

may be prohibitive. As a solution to this problem one can use a harmonic progression model to enhance the convergence.[23] Assuming that $N_i(E)$ has been computed for $i=1,n$, the contributions $N_i(E)$ $i=n+1\ldots\infty$ are estimated using a harmonic progression. The best estimate of the rate constant based on the data for the n lowest vibrational states of the activated complex then reads[23]

$$k_n(T) = \frac{Q_{\mathrm{TS}}\exp(-\beta E_1)}{2\pi\hbar Q_r}\frac{\int dE\left\{\sum_{i=1}^{n} N_i(E)\right\}\exp(-\beta E)}{\sum_{i=1}^{n}\exp(-\beta E_i)}, \tag{8}$$

where Q_{TS} is the partition function at the transition state in harmonic approximation and E_i is the energy of the ith vibrational state of the activated complex in harmonic approximation. Since

$$\lim_{n\to\infty}\sum_{i=1}^{n}\exp(-\beta E_i) = Q_{\mathrm{TS}}\exp(-\beta E_1), \tag{9}$$

$k_n(T)$ converges to the exact $k(T)$

$$\lim_{n\to\infty} k_n(T) = k(T). \tag{10}$$

If the harmonic approximation is reasonable, then Eq. (8) converges with a smaller number of thermal flux eigenstates than Eq. (7). It should be noted that the first factor on the right-hand side of Eq. (8) also appears in the harmonic TST. The thermal rate constant in harmonic TST reads

$$k^{\mathrm{TST}}(T) = \frac{1}{\beta}\frac{Q_{\mathrm{TS}}\exp(-\beta E_1)}{2\pi\hbar Q_r}. \tag{11}$$

Downloaded 07 Jun 2010 to 192.38.67.112. Redistribution subject to AIP license or copyright; see http://jcp.aip.org/jcp/copyright.jsp

B. The multiconfiguration time-dependent Hartree approach

The MCTDH approach is an efficient scheme to perform quantum calculations for high-dimensional systems.[77–80] In the MCTDH approach the wave function is represented as

$$\Psi(x_1 \ldots x_f,t) = \sum_{j_1=1}^{n_1} \ldots \sum_{j_f=1}^{n_f} A_{j_1 \ldots j_f}(t) \prod_{k=1}^{f} \phi_{j_k}^{(k)}(x_k,t). \quad (12)$$

The time-dependent basis functions $\phi_i^{(k)}(q_k,t)$, $k=1 \ldots f$ are called single-particle functions. The single-particle functions are expanded in time-independent bases $\chi_j^{(k)}(x_k)$

$$\phi_i^{(k)}(x_k,t) = \sum_{j=1}^{N_k} c_{ij}^{(k)}(t) \chi_j^{(k)}(x_k). \quad (13)$$

The equations of motion for the coefficients $A_{j_1 \ldots j_f}(t)$ and $c_{ij}^{(k)}(t)$ are derived from the Dirac–Frenkel variational principle. The MCTDH wave function converges towards the exact solution of the wave function if $n_i \rightarrow N_i$ and $N_i \rightarrow \infty$, for $i=1 \ldots f$.

In the present work, the MCTDH approach is utilized to perform all real and imaginary time propagations appearing in the flux correlation functions. A modified iterative Lanczos scheme as described in Ref. 81 is used to calculate the eigenstates of the thermal flux operator. For the real- or imaginary-time propagation a modified version of the constant mean-field integration scheme[82] has been employed. Matrix elements of the potential are calculated using the correlation-discrete variable representation approach.[83]

C. Shepard interpolation

An efficient procedure to construct multidimensional PESs is the Shepard interpolation scheme.[74,75] The potential at a point $\mathbf{Z}$ is given as a weighted average of local second-order Taylor expansions $V_i(\mathbf{Z})$ for different reference points $\mathbf{Z}_i$,

$$V(\mathbf{Z}) = \sum_i w_i(\mathbf{Z}) V_i(\mathbf{Z}). \quad (14)$$

$w_i(\mathbf{Z})$ weighs the contribution of the reference point $\mathbf{Z}_i$ and $V_i(\mathbf{Z})$ is given by

$$V_i(\mathbf{Z}) = V(\mathbf{Z}_i) + (\mathbf{Z}-\mathbf{Z}_i)^{\mathrm{T}} \mathbf{G}_{\mathbf{Z}_i} + (\mathbf{Z}-\mathbf{Z}_i)^{\mathrm{T}} \mathbf{H}_{\mathbf{Z}_i} (\mathbf{Z}-\mathbf{Z}_i). \quad (15)$$

$\mathbf{G}_{\mathbf{Z}_i}$ is the gradient (first derivatives of V to the coordinates $\mathbf{Z}$) and $\mathbf{H}_{\mathbf{Z}_i}$ is the Hessian (matrix of second derivatives to $\mathbf{Z}_i$) at point $\mathbf{Z}_i$. The number of reference points required to obtain an accurate potential depends on the choice of the coordinates $\mathbf{Z}$ and the weighing function. The optimal choice depends on the system.

III. N_2 ON A STEPPED Ru(0001) SURFACE

A. Density-functional theory calculations

The density-functional theory calculations presented here have been performed with the DACAPO code,[84] where the Kohn–Sham equations are solved in a plane-wave basis restricted by the kinetic-energy cutoff of 25 Ry. We employed revised Perdew–Burke–Ernzerhof (rPBE)[85] generalized gradient correction self-consistently, and the core electrons of both the Ru and N atoms were treated with Vanderbilt nonlocal ultrasoft pseudopotentials.[86] The sampling of six special k points was used together with a Fermi smearing of 0.1 eV. The Ru steps were modeled by using Ru(0001) and a (4×2) surface cell, where two atom rows were removed to give a step. The thickness of the slab was three layers. It has been shown that this gives a good description of N interaction with Ru(0001).[52] The transition state of N_2 dissociation was localized by constraining the N–N distance and relaxing the other nitrogen degrees of freedom. By varying the N–N distance, we localized the saddle point. We applied the same structure optimization procedure also for the other N–N distances on the minimum-energy path. The Hessian matrices needed for the interpolation of the potential-energy surface were obtained by displacing one N atom at a time in the three different Cartesian directions around the optimized configuration.

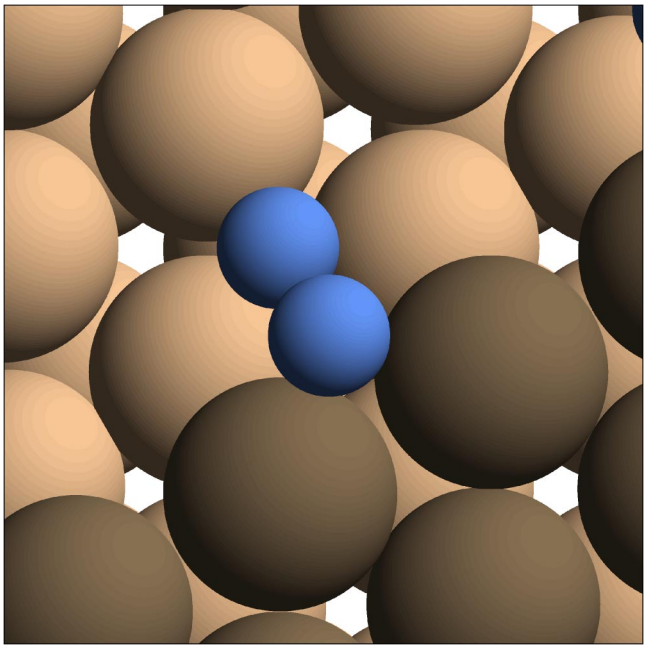

FIG. 1. The transition state for the dissociation of N_2. The big and small balls represent Ru and N atoms, respectively.

B. The Shepard interpolation procedure

Interpolation schemes based on inverse-bond distances[75] are favorable for many systems, since it automatically provides correct asymptotes and a correct description of the strong atom–atom repulsion at short atom–atom distances. A procedure to define bond lengths between molecular atoms and surface atoms in the Shepard interpolation approach is introduced by Crespos *et al.*[87,88]: the distances between the molecular atoms and the closest surface atoms are defined as bond lengths. For the present system, the upper and the lower N atoms have two and three close Ru neighbor atoms, respectively (see Fig. 1). Following the procedure of Crespos *et al.*,[87,88] we use these bond lengths in the interpolation scheme. Since the total number of bonds (five N–Ru bonds

Downloaded 07 Jun 2010 to 192.38.67.112. Redistribution subject to AIP license or copyright; see http://jcp.aip.org/jcp/copyright.jsp

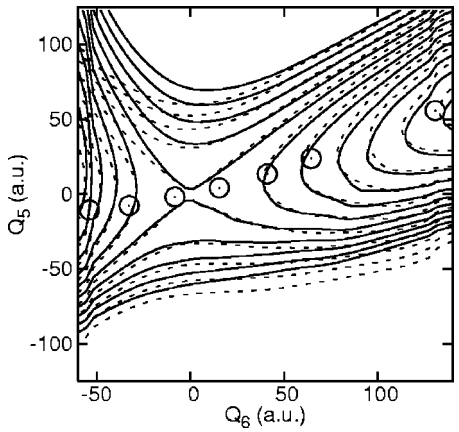

FIG. 2. The PES as a function of Q_5 and Q_6 ($Q_1 \ldots Q_4$ are relaxed). The equipotential lines are for energies between 0.7 and 1.2 eV, with a spacing of 0.05 eV. Solid lines: PES A (interpolation in inverse bond lengths). Dotted lines: PES B (interpolation in transition-state normal coordinates). Circles: positions of the reference points.

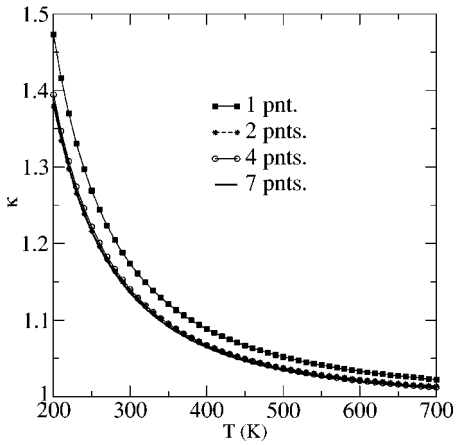

FIG. 3. $\kappa = k/k^{\mathrm{TST}}$ calculated using the various sets of reference points as indicated in Table I.

and one N–N bond) is equal to the number of degrees of freedom, gradients and Hessians in the inverse-bond coordinate system can be calculated straightforwardly from gradients and Hessians in Cartesian coordinates. A corresponding choice of the weighing function is used

$$w_i(\mathbf{Z}) = \frac{\|\mathbf{Z} - \mathbf{Z}_i\|^{-12}}{\sum_i \|\mathbf{Z} - \mathbf{Z}_i\|^{-12}}, \tag{16}$$

where $\mathbf{Z}$ are the inverse-bond distances.

For comparison, we also considered an interpolation procedure using transition-state normal coordinates for the second-order Taylor expansions [$V_i(\mathbf{Z})$ of Eq. (15)]. The two PESs obtained by the different interpolation schemes are called PES A (interpolation in inverse-bond distances) and PES B (interpolation in transition-state normal coordinates). Contour plots of the PESs as functions of the transition-state normal modes Q_5 and Q_6, with optimized coordinate values for $Q_1 \ldots Q_4$, are shown in Fig. 2 together with the positions of the reference points. Q_6, the reaction coordinate, mainly involves N–N stretching, and Q_5 mainly involves movements of N_2 perpendicular to the surface. Q_5 is the mode with the strongest coupling with the reactive mode Q_6. Figure 2 shows that PES A and PES B are very similar close to the minimum-energy path, but differ substantially further away from the reaction path.

C. Convergence with the number of reference points

The dominant computational effort in the present study are the DFT calculations of the Hessians at the reference points. It is therefore important to use the smallest possible number of reference points in the Shepard interpolation procedure. In the present study, only seven reference points on the minimum-energy path (MEP) have been considered. The reference points are obtained by optimizing the nitrogen degrees of freedom with the constraint that the N–N distance is fixed for a series of N–N distances (1.75, 1.85, 1.95, 2.05, 2.15, 2.25, and 2.5 Å). The positions of these points are shown graphically in Fig. 2. The point with a N–N distance of 1.95 Å is closest to the saddle point.

Comparing the results of quantum calculations (for details see Sec. III D) with different sets of reference points, one can see that even this small set of reference points is sufficient for accurate reaction-rate calculations. Because the differences between the calculated rate constants k are very small, it is more convenient to discuss the differences in the ratio $\kappa = k/k^{\mathrm{TST}}$, where k^{TST} is the thermal rate constant according to harmonic TST. Figure 3 presents κ calculated using the different sets of reference points defined in Table I. The differences between the results of the sets of two, four, and seven reference points are negligible. This indicates that only the reference points in a narrow range (1.9–2.1 Å) around the transition state are required. Even the result obtained with a single reference point differs with less than 6% from the seven-point result. It can therefore be expected that addition of more reference points on the MEP close to the transition state (N–N distances between 1.95 and 2.05 Å) would have a negligible effect on the reaction rate.

Although the potential is accurate close to the MEP, the potential should not be expected to be accurate in regions far from the MEP, where no reference points are available. PES A and PES B, obtained using different interpolation schemes, clearly differ in the region outside the reaction path. However, Fig. 4 shows that the difference between the results for κ obtained using PES A and PES B is small (less than 4%). Since the different treatment of anharmonicities in PES A and PES B does not effect the harmonic TST rate constant, comparison of the rate constant k yields the same result as the comparison of the κ factors. This suggests that the accu-

TABLE I. Sets of reference points for the interpolation of the potential.

Set	N–N distance (Å)						
1 point			1.95				
2 points			1.95	2.05			
4 points		1.85	1.95	2.05	2.15		
7 points	1.75	1.85	1.95	2.05	2.15	2.25	2.5

Downloaded 07 Jun 2010 to 192.38.67.112. Redistribution subject to AIP license or copyright; see http://jcp.aip.org/jcp/copyright.jsp

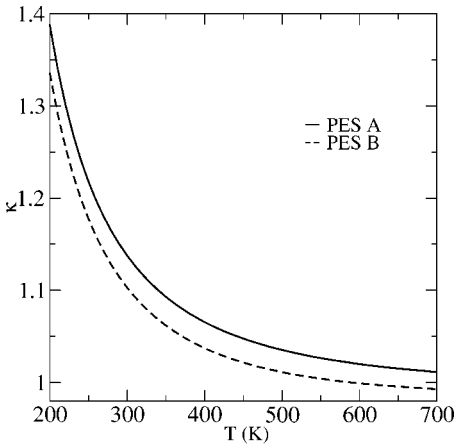

FIG. 4. $\kappa = k/k^{TST}$ for PES A and PES B.

racy of the PES in the region outside the reaction path is not crucial for the accuracy of reaction-rate calculations.

D. Quantum-dynamics calculations

The system is described using the six transition-state normal coordinates $Q_1 \ldots Q_6$, which form a convenient coordinate system to describe the dynamics in the vicinity of the transition state. Q_6, the mode with the imaginary frequency, can be considered as a reaction coordinate. The dividing surface is defined as $Q_6 = 0$. The Hamiltonian $\hat{H}$ in atomic units is given by

$$\hat{H} = -\sum_{i=1}^{6} \frac{\partial^2}{\partial Q_i^2} + V(Q_1, Q_2, \ldots, Q_6) - iW_{Q_6}, \tag{17}$$

where $V(Q_1, Q_2, \ldots, Q_6)$ is the PES and W_{Q_6} is a complex-absorbing potential (CAP). The construction of the PES is discussed in detail in Secs. III A–III C. The CAP (W_{Q_6}) is given by

$$W_{Q_6} = \begin{cases} k(Q_6 - Q_6^r)^2 & \text{if } Q_6 \geqslant Q_6^r, \\ k(Q_6 + Q_6^l)^2 & \text{if } Q_6 \leqslant Q_6^l, \\ 0 & \text{if } Q_6^l < Q_6 < Q_6^r. \end{cases} \tag{18}$$

Q_6^l and Q_6^r define the barrier region $Q_6^l \leqslant Q_6 \leqslant Q_6^r$. The values of Q_1^l and Q_6^r have been chosen so that the barrier region has a sufficient range to yield converged rate constants. The numerical parameters used in the converged quantum calculations are presented in Tables II and III.

TABLE II. Parameters for the MCTDH representation of the wave function.

Coordinate	Number of single-particle functions	Grid size	Grid type	Grid range (a.u.)
Q_1	3	30	Hermite DVR	
Q_2	3	32	Hermite DVR	
Q_3	3	33	Hermite DVR	
Q_4	3	35	Hermite DVR	
Q_5	3	96	FFT	−240–320
Q_6	4	192	FFT	−320–400

TABLE III. Numerical parameters used in the wave-packet propagation.

T_0 (Reference temp.)	300 K
Propagation time	73 fs
k	1.2×10^{-6} a.u.
Q_6^l	−80 a.u.
Q_6^r	160 a.u.

Several convergence tests have been carried out to ensure that the quantum-dynamics calculations are converged. One of these convergence test concerns the convergence with n, the number of activated states explicitly included in the calculation of k [Eq. (8)]. Figure 5 compares κ for $n = 1$, 6, and 21. The differences are negligible and converged results are already obtained for $n = 1$. This was also found in previous calculations for gas-phase systems.[22,23]

The rotational and vibrational partition functions of N_2 have been computed within the rigid rotor and the harmonic oscillator approximations, respectively. Relevant PES data obtained from DFT calculations are given in Table IV.

IV. RESULTS AND DISCUSSION

The Arrhenius plot of the rate constant obtained from quantum-mechanical calculations and harmonic TST is presented in Fig. 6. On the scale of this figure differences are hardly visible, even at the lowest temperatures (200 K). This figure clearly demonstrates that quantum effects on the reaction rate are small. The ratio between the accurate quantum rate constant $k(T)$ and the harmonic TST approximation $k^{TST}(T)$, $\kappa(T) = k(T)/k^{TST}(T)$ (which is often called tunneling factor), has already been presented in Fig. 5. From this figure one can find more detailed numbers; the enhancement due to quantum effects decreases from 40% at $T = 200$ K to 10% at room temperature. Thus, TST yields an adequate description at room temperature and gives a good approximation even at significantly lower temperatures.

More insight on the role of tunneling on the rate constant is obtained by studying the cumulative reaction probability

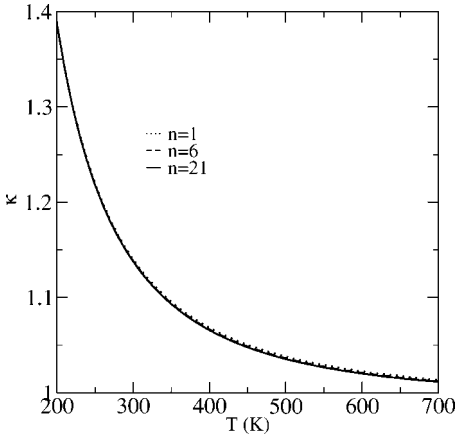

FIG. 5. $\kappa(T) = k/k^{TST}$ for various numbers n of vibrational states of the activated complex included in the calculation.

Downloaded 07 Jun 2010 to 192.38.67.112. Redistribution subject to AIP license or copyright; see http://jcp.aip.org/jcp/copyright.jsp

TABLE IV. Potential-energy surface data: The classical barrier height and harmonic frequencies at the transition state ($\omega_1-\omega_6$) and of isolated N_2 (ω).

Transition state	
Classical barrier	1.0 eV
ω_1	578 cm^{-1}
ω_2	517 cm^{-1}
ω_3	446 cm^{-1}
ω_4	423 cm^{-1}
ω_5	411 cm^{-1}
ω_6	409i cm^{-1}
Isolated N_2	
Geometry	2.12 a_0
ω	2492 cm^{-1}

$N(E)$. In TST, $N(E)$ is equal to the number of states of the activated complex with an energy less than E. Figure 7 shows the harmonic TST result together with the quantum result, displayed for an energy range relevant at room temperature. Note that the origin of the energy is the minimum of the potential energy of N_2 in the gas phase. The quantum result is in good overall agreement with the TST result. The only difference is that the steps are smoothened due to tunneling, which is most obviously demonstrated in the inset of Fig. 7. For most practical purposes, however, the tunneling can be neglected. At an energy of 0.1 eV below the threshold energy (1.15 eV), the reaction probability has already a value below 10^{-5}. This result is in sharp contrast to the results of previous model calculations of the dissociation probability for N_2 on various metal surfaces,[66–72] where significant reaction probabilities ($\approx 10^{-5}$) have been found for more than 0.3 eV below the barrier energy. Note that $N(E)$ is an upper bound to the initial state-selected reaction probabilities since it is the sum of all reaction probabilities.

In order to gain insight into the wave-packet dynamics, we discuss the time evolution of the thermal flux eigenstate which corresponds to the ground state of the activated complex with positive flux eigenvalue. This state will be denoted as $|f_1\rangle$ in the following. The wave packet is projected on the (Q_5,Q_6) plane. Q_6, the reaction coordinate, mainly involves N–N stretching, and Q_5 mainly involves movements of N_2 perpendicular to the surface. Q_5 is the mode with the strongest coupling with the reactive mode Q_6. Negative and positive values of Q_6 correspond to the reactant and product side, respectively. Figure 8 presents the probability density $\rho(Q_5,Q_6,t)$. Initially, the wave packet is localized around the transition-state region $Q_5=Q_6=0$. In the course of time almost the complete wave packet moves towards the product

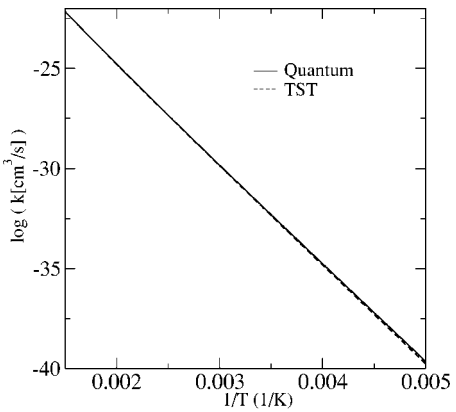

FIG. 6. Arrhenius plot of the thermal rate constants obtained from quantum-mechanical and TST calculations.

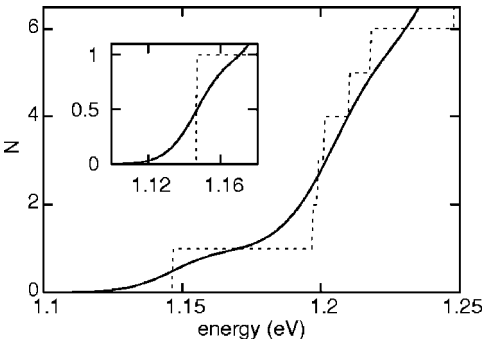

FIG. 7. The cumulative reaction probability as a function of the energy. Solid line: quantum result. Dashed line: TST result. The inset shows $N(E)$ in the threshold region.

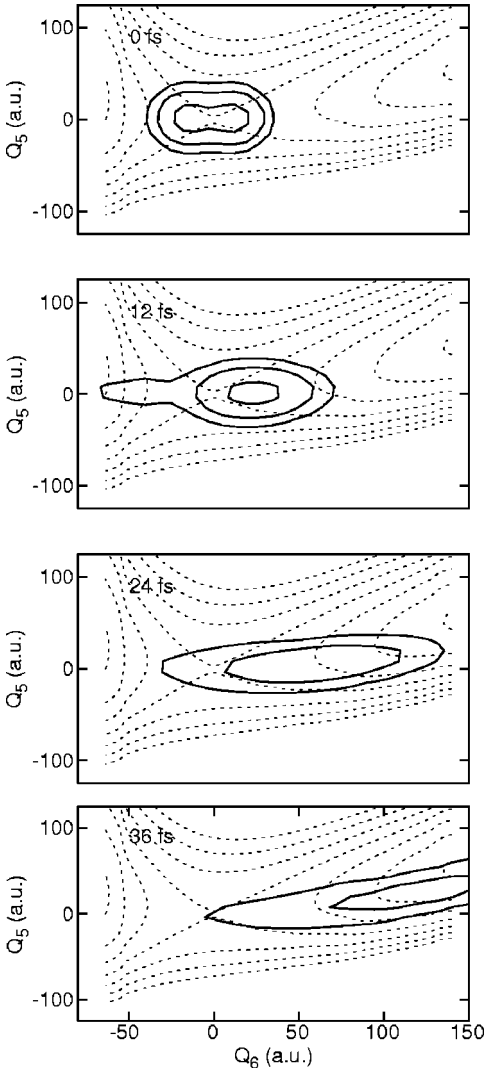

FIG. 8. Contour plot of the probability density $\rho(Q_5,Q_6,t)$ (see text) at different times as indicated in the figure. Solid lines: contours of the density. Dashed line: contour plot of the PES.

Downloaded 07 Jun 2010 to 192.38.67.112. Redistribution subject to AIP license or copyright; see http://jcp.aip.org/jcp/copyright.jsp

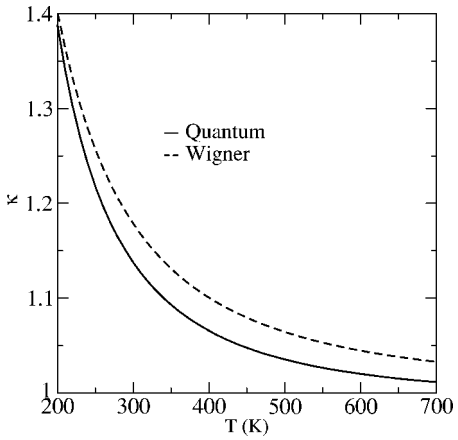

FIG. 9. $\kappa(T)=k/k^{\mathrm{TST}}$ obtained from accurate quantum-mechanical calculations and Wigner's tunneling theory.

side. Only a tiny part moves towards the reactant side, as revealed in the probability density for $t=12$ fs. After about 36 fs the wave packet has left the transition-state region. The other wave packets behave similarly; wave packets with positive flux eigenvalue move towards product region, while wave packets with a negative flux eigenvalue move towards the reactant region. Only tiny parts of the wave packet move towards other directions. This behavior can be explained by the small variations in the PES in the region where the initial wave packet is localized. In previous rate calculations involving hydrogen atoms,[21,24] the initial wave packets have a much larger extension relative to changes in the PES. Significant parts of the wave packets were thus located relatively far from the dividing surface, which explains the stronger recrossing behavior. The difference between H transfer reactions and the dissociation of N_2 is thus dominantly a mass effect. Because of the higher mass of nitrogen, the imaginary frequency ω_6 is much smaller for the present system. This results in a smaller relative width of the thermal flux eigenstates.

The Wigner tunneling correction factor[89] gives a direct relation between ω_6 and κ,

$$\kappa^{\mathrm{Wigner}} = 1 + \tfrac{1}{24}(\beta\hbar|\omega_6|)^2. \tag{19}$$

Since the Wigner correction factor is derived on the basis of a one-dimensional harmonic barrier model, it cannot describe deep tunneling. However, Fig. 9 shows that for the present case it is accurate even at low temperatures. The good agreement between the accurate quantum-mechanical result and the Wigner theory is a clear indication that the present system is close to the classical limit.

The obstinacy of tunneling theories in the literature for N_2 on a plain metal surfaces[66–72] is presumably caused by the experimental observation of significant reaction probabilities at energies well below the barrier energy. This observation could be explained by a tunneling mechanism. However, it is now known[63] that at low energies the reaction is dominated by step sites on the surface, where the barriers for dissociation are much lower. A tunneling mechanism is no longer required to explain the experimental findings. The strong tunneling effect found in the previous model calculations is presumably caused by an artificially narrow barrier in the model potential-energy surfaces employed. While the model calculations concern dissociation on plain surfaces and not on stepped surfaces as in the present study, there is no reason to expect a different behavior for dissociation on step sites than on the plain surface.

Although the present work gives an accurate six-dimensional (6D) quantum-dynamics study, the present rate constants cannot be compared directly with experimental results. In this work, the Ru surface is treated as a rigid surface. Relaxation of the positions of the ruthenium atoms results in a significant reduction of the barrier energy.[73] However, the ruthenium and nitrogen degrees of freedom are almost uncoupled in the barrier region. The topology of the PES in the barrier region is not significantly changed when the surface atoms are allowed to relax. Thus, the effect of the surface degrees of freedom is mainly an energy shift. Although this has a large effect on the magnitude of the reaction rate, it does not affect the reaction dynamics. Therefore the frozen-surface description allows for a reliable evaluation of quantum effects, which is the aim of the present work.

V. CONCLUSION

Approaches developed for gas-phase reaction-rate calculations have been applied successfully to a molecule–surface system: dissociative adsorption of N_2 on Ru. A potential-energy surface is constructed using density-functional theory calculations and Shepard interpolation. Reaction rates are then calculated using flux correlation functions and MCTDH wave-packet dynamics. Using this approach, the full-dimensional quantum dynamics of a heavy-diatom reaction on a surface could be described accurately. The effect of tunneling on the reaction rate is found to be almost negligible, which is in marked contrast to findings of previous model calculations.[66–68,70–72] Harmonic transition-state theory can be used to reliably predict the rate constant for dissociative adsorption of nitrogen on Ru and similar processes. While the present work has been restricted to a frozen Ru surface, future work[73] will include the effect of surface motion.

ACKNOWLEDGMENTS

The work is financially supported by the European Commission through the RTN Program Predicting Catalysis (HPRN-CT-2002-00170), the Deutsche Forschungsgemeinschaft, and by the Fond der Chemischen Industrie. K.H. acknowledges the computer resources from the Danish Center for Scientific Computing.

[1] T. Yamamoto, J. Chem. Phys. **33**, 281 (1960).
[2] W. H. Miller, J. Chem. Phys. **61**, 1823 (1974).
[3] W. H. Miller, S. D. Schwartz, and J. W. Tromp, J. Chem. Phys. **79**, 4889 (1983).
[4] W. H. Thompson and W. H. Miller, J. Chem. Phys. **106**, 142 (1997).
[5] B. Poirier, J. Chem. Phys. **108**, 5216 (1997).
[6] H. Wang, W. H. Thompson, and W. H. Miller, J. Chem. Phys. **107**, 7194 (1997).
[7] D. H. Zhang and J. C. Light, J. Chem. Phys. **106**, 551 (1996).
[8] D. H. Zhang, J. C. Light, and S.-Y. Lee, J. Chem. Phys. **109**, 79 (1998).
[9] J. C. Light and D. H. Zhang, Faraday Discuss. **110**, 105 (1998).
[10] U. Manthe, T. Seideman, and W. H. Miller, J. Chem. Phys. **99**, 10078 (1993).

Downloaded 07 Jun 2010 to 192.38.67.112. Redistribution subject to AIP license or copyright; see http://jcp.aip.org/jcp/copyright.jsp

[11] U. Manthe, T. Seideman, and W. H. Miller, J. Chem. Phys. **101**, 4759 (1994).
[12] F. Matzkies and U. Manthe, J. Chem. Phys. **106**, 2646 (1997).
[13] F. Matzkies and U. Manthe, J. Chem. Phys. **108**, 4828 (1998).
[14] U. Manthe and F. Matzkies, Chem. Phys. Lett. **282**, 442 (1998).
[15] F. Matzkies and U. Manthe, J. Chem. Phys. **110**, 88 (1999).
[16] F. Matzkies and U. Manthe, J. Chem. Phys. **112**, 130 (2000).
[17] U. Manthe and F. Matzkies, J. Chem. Phys. **113**, 5725 (2000).
[18] U. Manthe, W. Bian, and W. Werner, Chem. Phys. Lett. **313**, 647 (1999).
[19] F. Huarte-Larranaga and U. Manthe, J. Chem. Phys. **118**, 8261 (2003).
[20] F. Huarte-Larranaga and U. Manthe, J. Chem. Phys. **113**, 5115 (2000).
[21] F. Huarte-Larranaga and U. Manthe, J. Phys. Chem. A **105**, 2522 (2001).
[22] F. Huarte-Larranaga and U. Manthe, J. Chem. Phys. **116**, 2863 (2002).
[23] F. Huarte-Larranaga and U. Manthe, J. Chem. Phys. **117**, 4635 (2002).
[24] U. Manthe, J. Theor. Comput. Chem. **1**, 153 (2002).
[25] T. Wu and U. Manthe, Science **306**, 2227 (2004).
[26] G. J. Kroes, Prog. Surf. Sci. **60**, 1 (1999).
[27] G. J. Kroes, A. Gross, E. J. Baerends, M. Scheffler, and D. A. McCormack, Acc. Chem. Res. **35**, 193 (2002).
[28] A. Gross, S. Wilke, and M. Scheffler, Phys. Rev. Lett. **75**, 2718 (1995).
[29] A. Gross and M. Scheffler, Chem. Phys. Lett. **256**, 417 (1996).
[30] A. Gross and M. Scheffler, Chem. Phys. Lett. **263**, 567 (1996).
[31] A. Gross and M. Scheffler, Phys. Rev. B **57**, 2493 (1998).
[32] A. Gross, C. M. Wei, and M. Scheffler, Surf. Sci. **416**, L1095 (1998).
[33] A. Eichler, J. Hafner, A. Gross, and M. Scheffler, Chem. Phys. Lett. **311**, 1 (1999).
[34] A. Eichler, J. Hafner, A. Gross, and M. Scheffler, Phys. Rev. B **59**, 13297 (1999).
[35] A. Gross and M. Scheffler, Phys. Rev. B **61**, 8425 (2000).
[36] J. Q. Dai and J. C. Light, J. Chem. Phys. **107**, 1676 (1997).
[37] G. J. Kroes, E. J. Baerends, and R. C. Mowrey, Phys. Rev. Lett. **78**, 3583 (1997).
[38] G. J. Kroes, E. J. Baerends, and R. C. Mowrey, J. Chem. Phys. **107**, 3309 (1997).
[39] D. A. McCormack, G. J. Kroes, R. A. Olsen, E. J. Baerends, and R. C. Mowrey, J. Chem. Phys. **110**, 7008 (1999).
[40] D. A. McCormack, G. J. Kroes, R. A. Olsen, E. J. Baerends, and R. C. Mowrey, Phys. Rev. Lett. **82**, 1410 (1999).
[41] D. A. McCormack, G. J. Kroes, R. A. Olsen, J. A. Groeneveld, J. N. P. van Stralen, E. J. Baerends, and R. C. Mowrey, Faraday Discuss. **117**, 109 (2000).
[42] M. F. Somers, D. A. McCormack, G. J. Kroes, R. A. Olsen, E. J. Baerends, and R. C. Mowrey, J. Chem. Phys. **117**, 6673 (2002).
[43] M. F. Somers, S. M. Kingma, E. Pijper, G. J. Kroes, and D. Lemoine, Chem. Phys. Lett. **360**, 390 (2002).
[44] M. F. Somers, D. Lemoine, and G. J. Kroes, Chem. Phys. **304**, 59 (2004).
[45] M. F. Somers, R. A. Olsen, H. F. Busnengno, E. J. Baerends, and G. J. Kroes, J. Chem. Phys. **121**, 11379 (2004).
[46] E. Pijper, M. F. Somers, G. J. Kroes, R. A. Olsen, E. J. Baerends, H. F. Busnengo, A. Salin, and D. Lemoine, Chem. Phys. Lett. **347**, 277 (2001).
[47] E. Pijper, G. J. Kroes, R. A. Olsen, and E. Baerends, J. Chem. Phys. **117**, 5885 (2002).
[48] S. M. Kingma, M. F. Somers, E. Pijper, G. J. Kroes, R. A. Olsen, and E. J. Baerends, J. Chem. Phys. **118**, 4190 (2003).
[49] H. F. Busnengo, E. Pijper, G. J. Kroes, and A. Salin, J. Chem. Phys. **119**, 12553 (2003).
[50] J. K. Vincent, R. A. Olsen, G. J. Kroes, and E. J. Baerends, Surf. Sci. **573**, 433 (2004).
[51] R. van Harrevelt and U. Manthe, J. Chem. Phys. **121**, 3829 (2004).
[52] Á. Logadóttir, and J. K. Nørskov, J. Catal. **220**, 273 (2003).
[53] H. Shi, K. Jacobi, and G. Ertl, J. Chem. Phys. **99**, 9248 (1993).
[54] H. Dietrich, P. Geng, K. Jacobi, and G. Ertl, J. Chem. Phys. **104**, 375 (1996).
[55] M. J. Murphy, J. F. Skelly, A. Hodgson, and B. Hammer, J. Chem. Phys. **110**, 6954 (1999).
[56] S. Dahl, E. Törnqvist, and I. Chorkendorff, J. Catal. **192**, 381 (2000).
[57] L. Diekhöner, H. Mortensen, A. Baurichter, and A. C. Luntz, J. Chem. Phys. **115**, 3356 (2001).
[58] L. Diekhöner, H. Mortensen, A. Baurichter, E. Jensen, V. V. Pertunin, and A. C. Luntz, J. Chem. Phys. **115**, 9028 (2001).
[59] L. Diekhöner, L. Hornekaer, H. Mortensen, E. Jensen, A. Baurichter, V. V. Pertunin, and A. C. Luntz, J. Chem. Phys. **117**, 5018 (2002).
[60] H. Mortensen, E. Jensen, L. Diekhöner, A. Baurichter, A. C. Luntz, and V. V. Petrunin, J. Chem. Phys. **118**, 11200 (2003).
[61] J. J. Mortensen, Y. Morikawa, B. Hammer, and J. K. Nørskov, J. Catal. **169**, 85 (1997).
[62] J. J. Mortensen, B. Hammer, and J. K. Nørskov, Phys. Rev. Lett. **80**, 4333 (1998).
[63] S. Dahl, Á. Logadóttir, R. C. Egeberg, J. H. Larsen, I. Chorkendorff, E. Törnqvist, and J. K. Nørskov, Phys. Rev. Lett. **83**, 1814 (1999).
[64] T. H. Rod, Á. Logadóttir, and J. K. Nørskov, J. Chem. Phys. **112**, 5343 (2000).
[65] K. Honkala, A. Hellman, I. N. Remediakis, Á. Logadóttir, A. Carlsson, S. Dahl, C. H. Christensen, and J. K. Nørskov, Science **307**, 5709 (2005).
[66] S. Holloway, D. Halstead, and A. Hodgson, J. Electron Spectrosc. Relat. Phenom. **45**, 207 (1987).
[67] G. Haase, M. Asscher, and R. Kosloff, J. Chem. Phys. **90**, 3346 (1989).
[68] G. D. Billing, A. Guldberg, N. E. Henriksen, and F. Y. Hansen, Chem. Phys. **147**, 1 (1990).
[69] F. Y. Hansen, N. E. Henriksen, and G. D. Billing, Surf. Sci. **324**, 55 (1995).
[70] L. Romm, G. Katz, R. Kosloff, and M. Asscher, J. Phys. Chem. B **101**, 2213 (1997).
[71] L. Romm, O. Citri, R. Kosloff, and M. Asscher, J. Chem. Phys. **112**, 8821 (2000).
[72] N. E. Henriksen, F. Y. Hansen, and G. D. Billing, Chem. Phys. Lett. **330**, 139 (2000).
[73] R. van Harrevelt, K. Honkala, J. K. Nørskov, and U. Manthe (unpublished).
[74] K. C. Thompson, M. J. T. Jordan, and M. A. Collins, J. Chem. Phys. **108**, 564 (1998).
[75] K. C. Thompson, M. J. T. Jordan, and M. A. Collins, J. Chem. Phys. **108**, 8302 (1998).
[76] T. Wu and U. Manthe, J. Chem. Phys. **119**, 14 (2003).
[77] H.-D. Meyer, U. Manthe, and L. S. Cederbaum, Chem. Phys. Lett. **165**, 73 (1990).
[78] U. Manthe, H.-D. Meyer, and L. S. Cederbaum, J. Chem. Phys. **97**, 3199 (1992).
[79] M. H. Beck, A. Jäckle, G. A. Worth, and H.-D. Meyer, Phys. Rep. **324**, 1 (2000).
[80] H.-D. Meyer and G. A. Worth, Theor. Chem. Acc. **109**, 251 (2003).
[81] U. Manthe and F. Matzkies, Chem. Phys. Lett. **252**, 7 (1996).
[82] M. H. Beck and H.-D. Meyer, Z. Phys. D: At., Mol. Clusters **42**, 113 (1997).
[83] U. Manthe, J. Chem. Phys. **105**, 6989 (1996).
[84] http://www.fysik.dtu.dk/campos/Dacapo/
[85] B. Hammer, L. B. Hansen, and J. K. Nørskov, Phys. Rev. B **59**, 7413 (1999).
[86] D. Vanderbilt, Phys. Rev. B **41**, 7892 (1990).
[87] C. Crespos, M. A. Collins, E. Pijper, and G. J. Kroes, Chem. Phys. Lett. **376**, 566 (2003).
[88] C. Crespos, M. A. Collins, E. Pijper, and G. J. Kroes, J. Chem. Phys. **120**, 2392 (2004).
[89] E. Wigner, Z. Phys. Chem. B. **19**, 203 (1932).

Downloaded 07 Jun 2010 to 192.38.67.112. Redistribution subject to AIP license or copyright; see http://jcp.aip.org/jcp/copyright.jsp